Popel, A., Adamska, A. M., Martin, P. G., Payton, O. D., Lampronti, G. I., Picco, L., ... Farnan, I. (2016). Structural effects in UO_2 thin films irradiated with U ions. *Nuclear Instruments and Methods in Physics Research, Section B: Beam Interactions with Materials and Atoms*, *386*, 8-15. https://doi.org/10.1016/j.nimb.2016.09.019

Nuclear Instruments and Methods in Physics Research B 386 (2016) 8–15

Contents lists available at ScienceDirect

Nuclear Instruments and Methods in Physics Research B

journal homepage: www.elsevier.com/locate/nimb

Structural effects in UO_2 thin films irradiated with U ions

A.J. Popel [a,*], A.M. Adamska [b], P.G. Martin [b], O.D. Payton [b], G.I. Lampronti [a], L. Picco [b], L. Payne [b], R. Springell [b], T.B. Scott [b], I. Monnet [c], C. Grygiel [c], I. Farnan [a]

[a] Department of Earth Sciences, University of Cambridge, Downing Street, Cambridge CB2 3EQ, United Kingdom
[b] Interface Analysis Centre, School of Physics, University of Bristol, Bristol BS8 1TL, United Kingdom
[c] CIMAP, CEA-CNRS-ENSICAEN-Université de Caen, BP 5133, 14070 Caen Cedex5, France

ARTICLE INFO

Article history:
Received 7 June 2016
Received in revised form 29 July 2016
Accepted 18 September 2016

Keywords:
UO_2
Single crystal
Ion irradiation
Thin film
Nano-structure
EBSD

ABSTRACT

This work presents the results of a detailed structural characterisation of irradiated and unirradiated single crystal thin films of UO_2. Thin films of UO_2 were produced by reactive magnetron sputtering onto (0 0 1), (1 1 0) and (1 1 1) single crystal yttria-stabilised zirconia (YSZ) substrates. Half of the samples were irradiated with 110 MeV $^{238}U^{31+}$ ions to fluences of 5×10^{10}, 5×10^{11} and 5×10^{12} ions/cm^2 to induce radiation damage, with the remainder kept for reference measurements. It was observed that as-produced UO_2 films adopted the crystallographic orientation of their YSZ substrates. The irradiation fluences used in this study however, were not sufficient to cause any permanent change in the crystalline nature of UO_2. It has been demonstrated that the effect of epitaxial re-crystallisation of the induced radiation damage can be quantified in terms of kernel average misorientation (KAM) and different crystallographic orientations of UO_2 respond differently to ion irradiation.

1. Introduction

The heat generated in a nuclear reactor comes primarily from the slowing down of fission products, which possess large energies in the range 70–100 MeV and produce heat and radiation damage inside the fuel matrix, leading to degradation of the fuel's properties [1–3]. Uranium dioxide, UO_2, a ceramic with a melting point of ~3150 K, is the main form of nuclear fuel used in the present generation of nuclear reactors [2]. As a result, extensive work is devoted to understanding the effect of radiation damage by fission fragments within the fuel on its structural and thermal performance with the aim of safe extension of the fuel burnup [1–10] and, to a lesser extent, on its chemical alteration and reactivity with water, which is relevant for subsequent spent fuel storage and disposal [11–14]. The knowledge and understanding of the fuel's in-reactor behaviour and its stability under subsequent storage and disposal conditions are of great technological importance [15,16].

This work considers the explicit effect of radiation damage on the structural integrity of UO_2, via single crystal UO_2 thin films with the three primary crystallographic orientations: (0 0 1), (1 1 0) and (1 1 1). For this purpose, the UO_2 films were produced on yttrium stabilised zirconia (YSZ) substrates with half of the samples irradiated with $^{238}U^{31+}$ ions of energies of 110 MeV to fluences of 5×10^{10}, 5×10^{11} and 5×10^{12} ions/cm^2 to mimic the radiation damage produced in nuclear fuel by the fission fragments. The irradiated and unirradiated films were characterised using a range of analytical techniques including: X-ray diffraction (XRD), electron backscatter diffraction (EBSD), scanning electron microscopy (SEM), high-speed atomic force microscopy (HS-AFM), dual beam (focused ion beam (FIB) and SEM), secondary ion mass spectrometry (SIMS) and energy dispersive X-ray (EDX) spectroscopy.

2. Experimental

2.1. Sample production

The single crystal thin film samples of UO_2 were produced so that each sample could provide different crystallographic orientations for the irradiation by the high-energy ion beam. It was known from the work by Strehle et al. [17], that high quality single crystal UO_2 films in (0 0 1) crystallographic orientation can be grown on (0 0 1) YSZ by direct current magnetron sputtering despite a −6.4% lattice mismatch between the UO_2 and YSZ lattices. At room temperature YSZ has a cubic fluorite structure with $a_{YSZ} = 5.139$ Å [17], with UO_2 having a cubic fluorite structure with $a_{UO_2} = 5.469$ Å [18]. This results in the plane-to-plane epitaxial match in which the (0 0 1) plane of UO_2 is put at a compressive

* Corresponding author.
E-mail address: apopel@cantab.net (A.J. Popel).

http://dx.doi.org/10.1016/j.nimb.2016.09.019
0168-583X/

strain of −6.4% by the (0 0 1) plane of YSZ. Since the lattice mismatch for (1 1 0)/(1 1 0) and (1 1 1)/(1 1 1) planes of UO_2 and YSZ is the same as for (0 0 1) planes, it was assumed that it will be possible to produce single crystal UO_2 that mimics the crystallographic orientation of the underlying YSZ substrate.

Six films of UO_2 (Table 1) were produced by reactive magnetron sputtering onto (0 0 1), (1 1 0) and (1 1 1) YSZ substrates at University of Bristol [18]. The substrates were one side polished single crystal YSZ (8 mol% Y_2O_3) 10 × 10 × 0.5 mm supplied by MTI Corp, USA. A dedicated direct current magnetron sputtering facility with ultra high vacuum base pressure (10^{-9} mbar) was used [19]. A depleted uranium metal target was used as a source of uranium, with the magnetron gun was kept at a power of 50 W by controlled direct current at an average value of 0.15 A and corresponding voltage of 330 V, giving a growth rate of ca. 1.5 Å/s. Argon was used as the sputtering gas at a p_{Ar} of ~8×10^{-3} mbar. Oxygen was used as the reactive gas at a p_{O_2} of 2×10^{-5} mbar for all samples (p_{O_2} of 3×10^{-6} mbar for sample SN553). The substrates were all kept at a temperature close to 600 °C for production of the samples.

2.2. Sample irradiation

Ion irradiation was conducted to simulate the expected radiation damage produced by fission fragments in a nuclear reactor fuel. For this purpose, half of the produced UO_2 samples (Table 1) were irradiated with 110 MeV energy $^{238}U^{31+}$ ions to fluences of 5×10^{10}, 5×10^{11} and 5×10^{12} ions/cm^2 respectively on the IRRSUD beamline at the GANIL accelerator, Caen, France. The remaining samples were kept in order to provide reference characterisation. Thin films with different crystallographic orientations were irradiated to different fluences due to limited number of samples.

The beamline base vacuum was 6×10^{-7} mbar during the sample irradiations. The flux was kept constant at ca. 1×10^8 ions/(cm^2 s). The irradiation was conducted at an ambient temperature of 16–17 °C, with no heating of the samples observed during this time. The ion beam was swept across the surface of the samples with a frequency of 400 Hz in the horizontal direction and 4 Hz in the vertical direction to ensure homogenous irradiation.

According to the SRIM-2013.00 software [20], the expected nuclear and electronic stopping, dE/dx, for 110 MeV U ions in UO_2 is 0.96 and 27.4 keV/nm, respectively, with the projected range at 6.7 μm. A theoretical UO_2 density of 10.96 g/cm^3 [3] was assumed in this SRIM calculation. The SRIM results indicate that the U ions completely penetrate the UO_2 film (150 nm max) and the electronic stopping regime dominates the dissipation of ion energy throughout the entire film.

2.3. Sample characterisation

The thickness of the films was measured using a coupled SEM and FIB (dual beam) setup and the results verified using a SIMS technique. The dual beam measurement was performed following the deposition of a protective platinum strip to act as an impingement plate (Fig. 1) followed by the ion milling to a depth of 2–3 μm using Ga^+ ions (30 keV, 6.5 nA). The thickness of the revealed UO_2 film was measured using high magnification SEM. The FIB was an FEI FIB Strata 201 and the SEM was an FEI Helios NanoLab 600. Ga^{1+} ions with energy of 25 keV at an incidence angle of 45° were used in the SIMS study. The beam current used during the operation remained relatively constant at 1 nA. The sample stage was kept at 3.93 kV. The sputtering rate for UO_2 was estimated to be 0.3 nm/s based on the sputter ratio obtained from the SRIM-2013.00 software. The SIMS study also allowed to assess stability of the film-substrate interface before and after the irradiation.

The surface morphology of the films was examined by means of high resolution SEM (FEI Helios NanoLab 600) and high-speed AFM (HS-AFM). The contact mode HS-AFM used in this work was custom built at the University of Bristol [21,22].

Surface composition was examined using EDX. An Octane-Plus™ silicon drift EDS detector with accompanying TEAM analytical software from EDAX was used. Throughout, a consistent 20 kV accelerating voltage, 120 μm aperture and 2.3 nA current were used. The samples were positioned horizontally at a working distance of 9 mm, to ensure maximum count rates were received by the detector.

The crystallographic orientations of the as-produced UO_2 films and the effect of the irradiation damage on UO_2 single crystal morphology were characterised using XRD and EBSD techniques. A D8 Bruker diffractometer equipped with a primary Ge monochromator for Cu Kα1 and a Sol-X solid state detector operating in

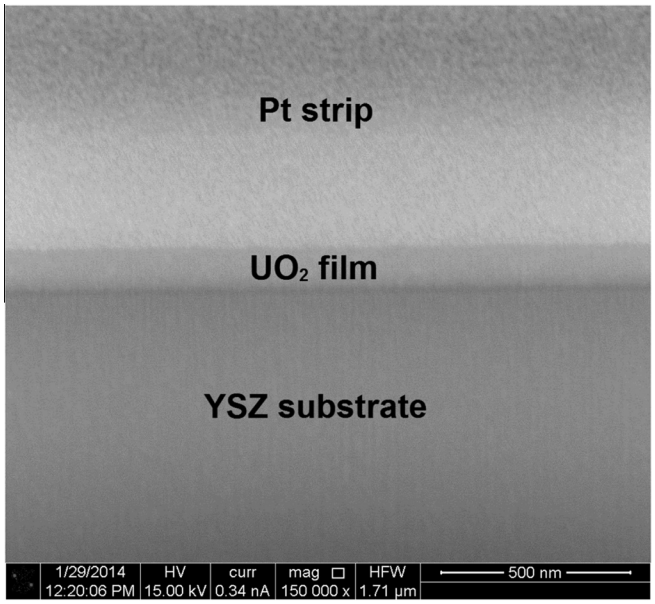

Fig. 1. A secondary electron SEM image of the film cross section cut with FIB for sample SN553* (UO_2 film on YSZ (1 1 0) irradiated to a fluence of 5×10^{11} U ions/cm^2). UO_2 film can be clearly seen in the middle.

Table 1
Summary of the EBSD results for thin films of UO_2 on YSZ substrates: (*hkl*) of as-produced and irradiated UO_2 films on YSZ substrates and the corresponding average values of kernel average misorientation angle.

Sample name	YSZ substrate (*hkl*)	UO_2 film (*hkl*)	Fluence (ions/cm^2)	Average value of kernel average misorientation angle (°)
SN551*	(0 0 1)	(0 0 1)	5×10^{10}	0.3
SN552	(0 0 1)	(0 0 1)	0	0.2
SN553*	(1 1 0)	(1 1 0)	5×10^{11}	0.8
SN554	(1 1 0)	(1 1 0)	0	0.2
SN556*	(1 1 1)	(1 1 1)	5×10^{12}	0.7
SN557	(1 1 1)	(1 1 1)	0	0.2

standard Bragg-Brentano geometry was used for the XRD analysis. EBSD instrumentation from AMETEK-EDAX associated with a Carl Zeiss Sigma™ Variable Pressure SEM fitted with a Gemini™ field emission electron column and Digiview 3 high speed camera were used.

No conductive film coating was used to preserve the surface of the samples for other studies. A conductive bridge was formed with a silver paste between the surface of the samples and the sample stage to mitigate sample charging.

3. Results

3.1. Film thickness

Film thickness is one of the key parameters for thin films and was measured using a combination of focused ion beam milling and scanning electron microscope imaging. The dual beam measurements performed for irradiated samples SN553* (* denotes irradiated samples) and SN556* indicated that the films had thicknesses of 145–150 nm. The film thickness for samples SN551, SN554 and SN557 was assumed to be the same as for samples SN553 and SN556, as the films were deposited for the same amount of time (1000 s), except for sample SN552 (600 s), under similar conditions. This results in the average film growth rate of 1.5 Å/s and gives an estimated film thickness for sample SN552 of ~90 nm. During the dual beam study it was impossible to resolve between the UO_2 film and the substrate for unirradiated sample SN554, possibly, due to a low electrical conductivity of the UO_2 film.

Verification by the SIMS technique resulted in the film thicknesses for samples SN553* and SN554 to be approximately 160 nm (Fig. 11), which is in good agreement with dual beam measurements.

3.2. Surface topography and composition

As no conductive coating was used and UO_2 has a low electric conductivity [23], the unirradiated films exhibited severe surface charging. As a result, difficulties were encountered in producing resolved images of the unirradiated samples. The only exception was sample SN554, where regular nano-scale ripples could be seen (Fig. 2) similar to those observed in work by Bao et al. [18] for a UO_2 film grown on a $LaAlO_3$ substrate.

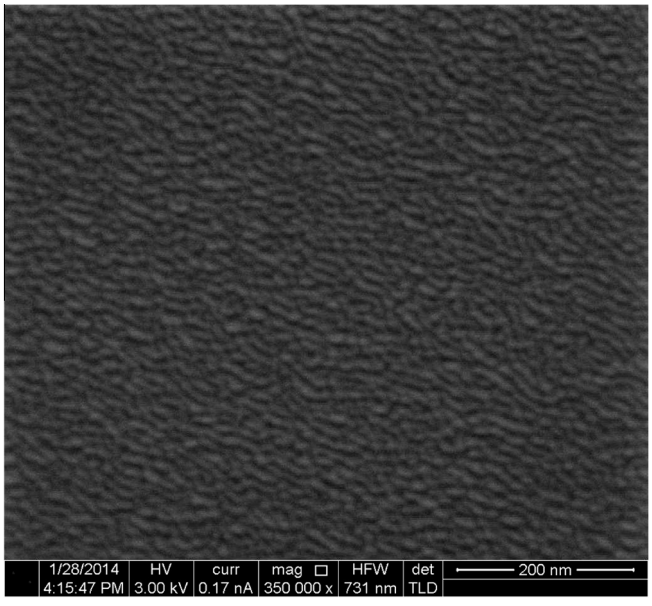

Fig. 2. A secondary electron SEM image of the surface topology of sample SN554 (unirradiated UO_2 film on YSZ (1 1 0)). Note nano-scale regular wave pattern.

High speed AFM study shows that the unirradiated films all have flat surfaces (Fig. 3a) with root mean square (RMS) roughness values of 2.0, 1.4 and 1.0 nm for samples SN552, SN554 and SN557, correspondingly.

In contrast, the irradiated samples were less prone to surface charging during SEM imaging. Hence, it was easier to produce well-resolved images (Fig. 4). Sample SN551* (Fig. 4a) shows a grain structure with a rectangular shape and dimensions ~30–40 nm × 5 nm and circular features with a diameter ~10 nm. Sample SN553* (Fig. 4b) shows regular nano-scale ripples similar to the ones observed in sample SN554 (Fig. 2) and circular features similar to the ones observed in sample SN551* with a diameter ~10 nm. Sample SN556* (not shown) shows similar features to sample SN551* – shorter and slightly wider rectangular shape grain structure with dimensions ~10–20 nm × 6 nm and circular features similar to the ones observed in samples SN551* and SN553* with a diameter ~10 nm. SEM images taken at an angle of 52° (not shown) to the surface of the irradiated samples show hillock features with diameters in the range 10–15 nm, i.e., ~5 times greater than the expected track diameter for U in UO_2. They also become more densely populated going from sample SN551* to SN556* following the increasing irradiation fluence trend, but not in direct proportion to the fluence.

High-speed AFM study showed that the ion irradiations resulted in hillock features with heights in the region of 10 nm (Fig. 3b). The root mean square roughness values increased to 4.4 (by 120%), 7.6 (by 450%) and 4.9 nm (by 390%) for samples SN551*, SN553* and SN556*, correspondingly.

A contaminant film was observed on the UO_2 surface for all samples during the HS-AFM study. The results of the EDX and X-ray photoelectron spectroscopy (XPS) [24] studies indicate that this film is carbonaceous in nature.

Micron and sub-micron scale contamination particles were also observed at the surface of the films.

The EDX setup used to analyse the films had a sampling depth of ~2 μm. Since the thickness of the films is only ~150 nm, the EDX signal contained a significant contribution from the substrate elements. Hence, it was not possible to perform sensitive analysis of the film composition on the surface. However, some useful information could still be obtained. EDX point analysis on the surface of the films free from particulate contamination provided two observations: 1) high level of carbon contamination – 30–45 atomic %; 2) high signal contribution from the substrate elements. When the analysis point was located at a contaminant particle on the surface of the film, it indicated that the particle mainly consists of oxides of U, Ta and Nb. Carbon contamination was observed again. The XPS study confirms the presence of carbon and niobium contamination.

3.3. Crystallographic structure

Results of the XRD studies for the unirradiated samples indicated that, in the employed experimental geometry, sample SN552 (Fig. 5) has three peaks from the UO_2 film which can be identified as 200, 400 and 600 reflections. Sample SN554 showed 220 and 440 UO_2 reflections (Fig. 6). The diffraction pattern from sample SN557 shows 111, 222 and 333 UO_2 reflections (Fig. 7).

EBSD was used to complement the XRD analysis of the UO_2 films. It allows the crystallographic orientation of microstructures on the surface of material to be determined [25]. The inverse pole figure (IPF) maps represent the crystallographic orientation of the scanned points on the surface of material (Fig. 8 left). The inverse pole figure triangular diagrams represent the distribution of the

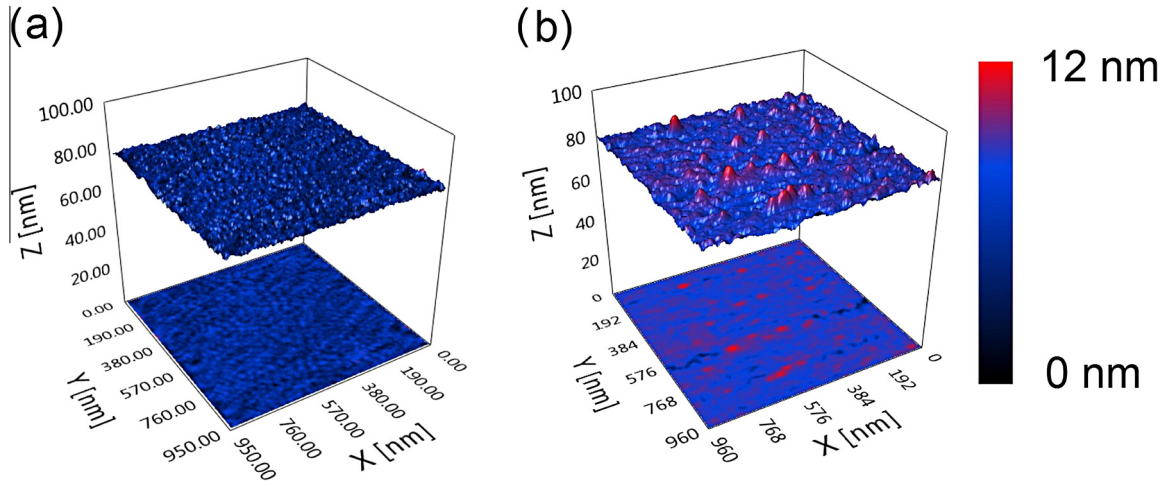

Fig. 3. 3D surface topography and its projection obtained by HSAFM for (a) unirradiated sample SN552 (UO_2 film on YSZ (0 0 1)) and (b) the corresponding irradiated (5×10^{10} ions/cm^2) sample SN551*.

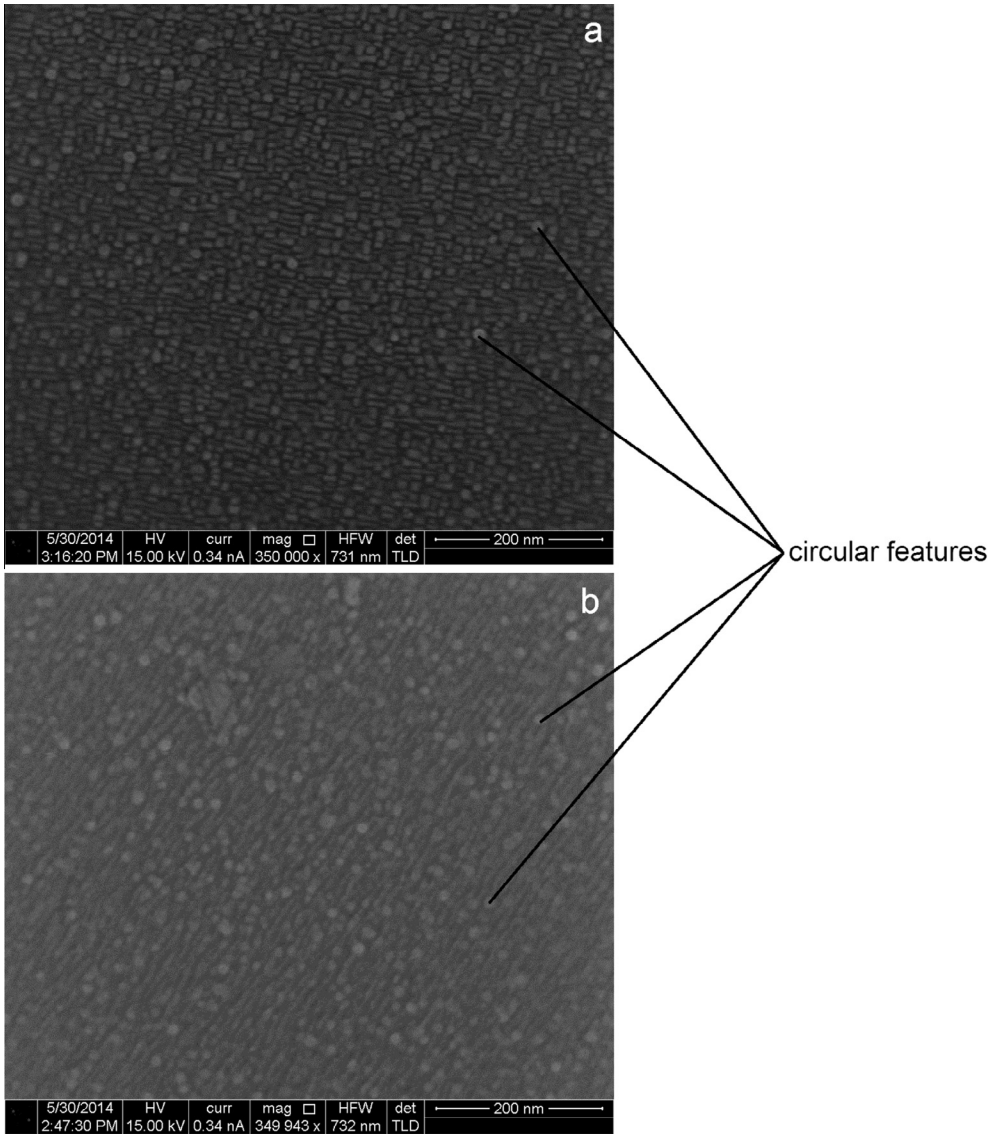

Fig. 4. SEM images taken perpendicular to the surface of the irradiated samples: (a) SN551* (UO_2 film on YSZ (0 0 1), 5×10^{10} ions/cm^2); (b) SN553* (UO_2 film on YSZ (1 1 0), 5×10^{11} ions/cm^2).

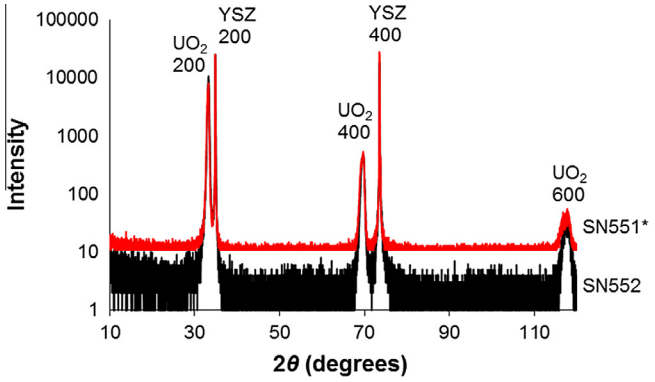

Fig. 5. XRD results for samples SN551* (irradiated UO_2 film on YSZ (0 0 1), 5×10^{10} ions/cm^2) and SN552 (unirradiated UO_2 film on YSZ (0 0 1)). XRD intensity for irradiated sample SN551* is shifted upwards for clarity.

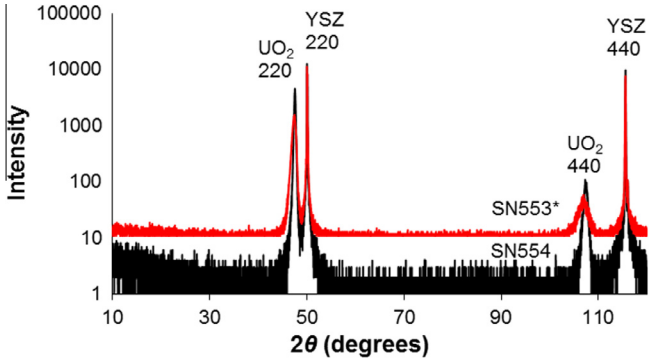

Fig. 6. XRD results for samples SN553* (irradiated UO_2 film on YSZ (1 1 0), 5×10^{11} ions/cm^2) and SN554 (unirradiated UO_2 film on YSZ (1 1 0)). XRD intensity for irradiated sample SN553* is shifted upwards for clarity.

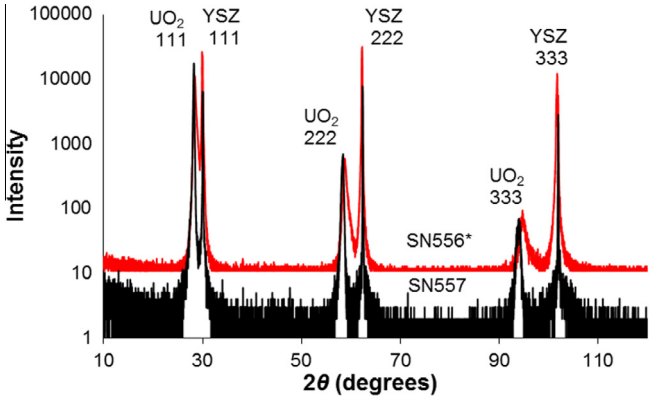

Fig. 7. XRD results for samples SN556* (irradiated UO_2 film on YSZ (1 1 1), 5×10^{12} ions/cm^2) and SN557 (unirradiated UO_2 film on YSZ (1 1 1)). XRD intensity for irradiated sample SN556* is shifted upwards for clarity.

scanned points on the surface of material in accordance to their crystallographic orientation (Fig. 8 right). The inverse pole figures from the EBDS study of samples SN552, SN554 and SN557 indicated that the surface of these samples has (0 0 1), (1 1 0) and (1 1 1) crystallographic orientation, respectively (Fig. 8). The EBSD results are summarised in Table 1. The EBSD technique allows also quantifying local misorientation in terms of kernel average misorientation (KAM) [25,26]. This method quantifies the average misorientation between a point on the measurement grid and its neighbours [25] and is characterised by an average misorientation

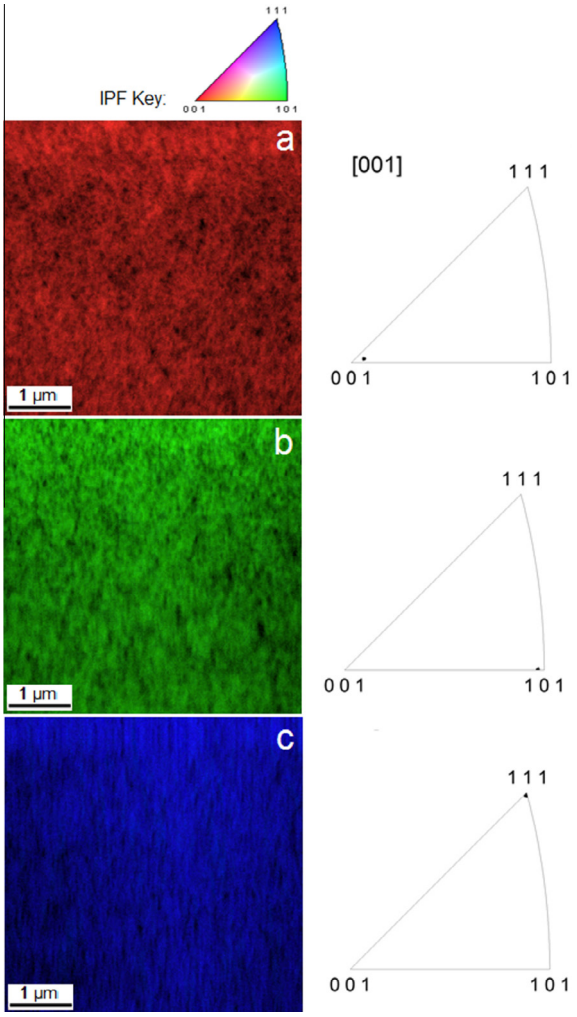

Fig. 8. Image quality and the inverse pole figure overlapped maps and the corresponding triangular IPF diagrams for unirradiated samples: (a) SN552 (UO_2 film on YSZ (0 0 1)); (b) SN554 (UO_2 film on YSZ (1 1 0)); (c) SN557 (UO_2 film on YSZ (1 1 1)).

angle. Kernel average misorientation is generally high in deformed regions due to higher dislocation density, local lattice distortions and localised deformation [26]. Hence, KAM was also used to assess the effect of the ion irradiations on structural alternations in the films.

From the XRD data for the irradiated samples it becomes evident that the ion irradiations did not result in any noticeable structural rearrangements. The diffraction pattern from sample SN551* (5×10^{10} ions/cm^2) showed virtually no noticeable changes from what was observed for the corresponding unirradiated sample SN552 (Fig. 5). Sample SN553* (5×10^{11} ions/cm^2) showed (Fig. 6) minor UO_2 peak broadening with slight shift towards lower values of 2θ, as compared to the corresponding unirradiated sample SN554. The substrate reflections remained virtually unchanged. The most profound UO_2 peak broadening and shift towards higher values of 2θ after irradiation was observed for sample SN556* (5×10^{12} ions/cm^2), as compared to the corresponding unirradiated sample SN557 (Fig. 7). For sample SN556* reflections from the substrate showed minor peak broadening with slight shift towards lower values of 2θ.

The inverse pole figure maps from the EBSD study also indicated that the irradiation even to the greatest ion fluence of 5×10^{12} ions/cm^2 did not cause any noticeable restructuring, with

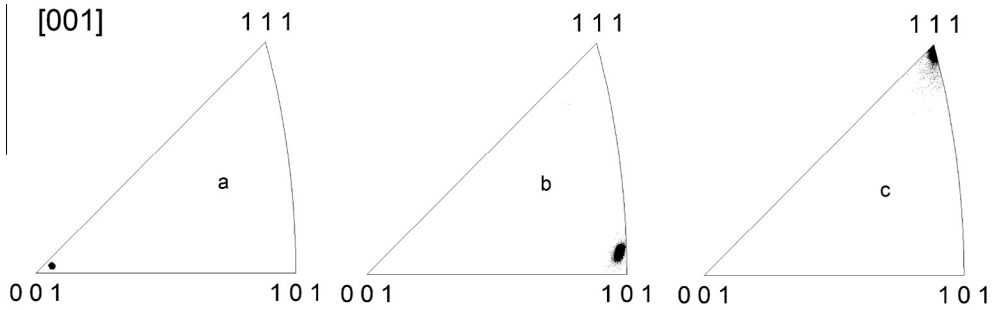

Fig. 9. The triangular inverse pole figure diagrams for irradiated samples: (a) SN551* (UO_2 film on YSZ (0 0 1), 5×10^{10} ions/cm^2); (b) SN553* (UO_2 film on YSZ (1 1 0), 5×10^{11} ions/cm^2); (c) SN556* (UO_2 film on YSZ (1 1 1), 5×10^{12} ions/cm^2).

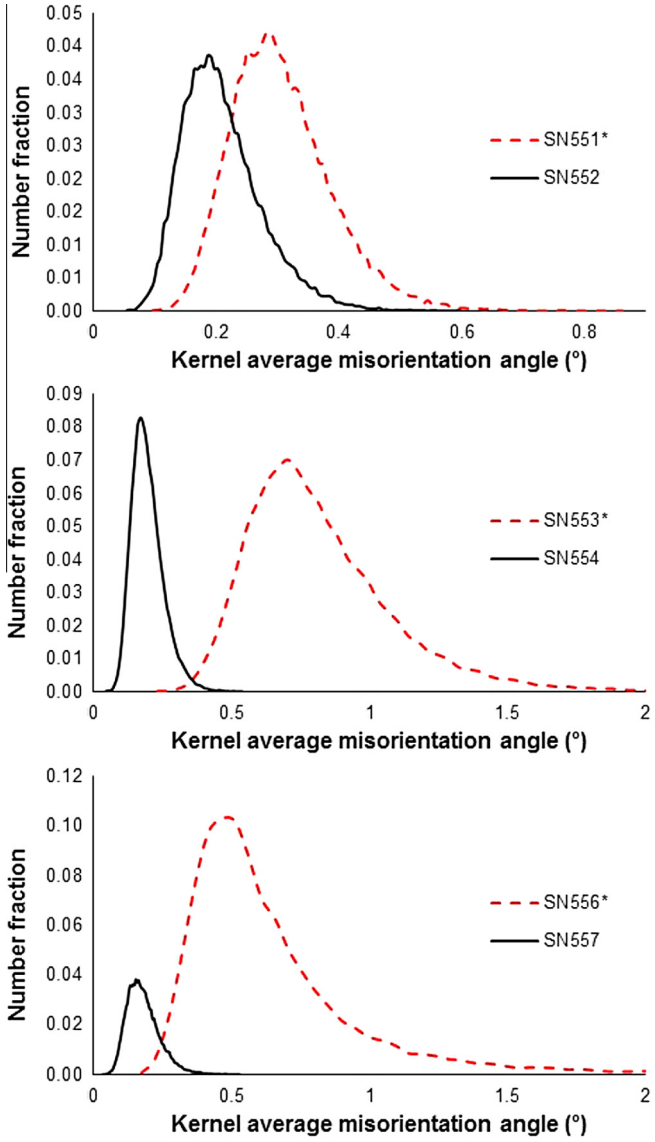

Fig. 10. Plots of number fraction for the corresponding values of kernel average misorientation for the irradiated and the corresponding unirradiated UO_2 films.

the irradiated samples retaining their crystallographic orientation. However, the triangular IPF diagrams (Fig. 9) showed more scatter for the irradiated samples in contrast to the corresponding unirradiated ones (Fig. 8 right). Hence, some degree of restructuring was taking place as a result of the ion irradiation.

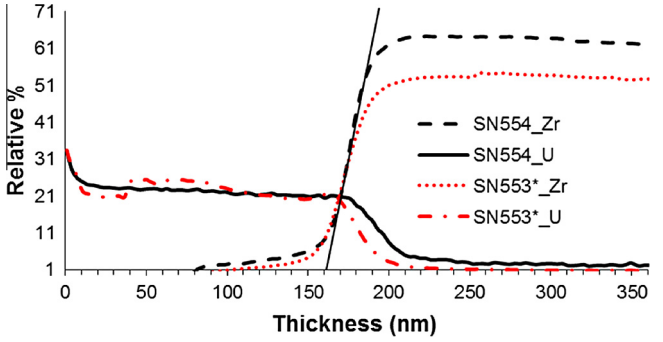

Fig. 11. A plot of the SIMS results for U-Zr pair for samples SN553* (irradiated UO_2 film on YSZ (1 1 0), 5×10^{11} U ions/cm^2) and SN554 (unirradiated UO_2 film on YSZ (1 1 0)). U is the film element and Zr is the substrate element.

Plots of number fraction for the corresponding values of KAM (Fig. 10) suggested that the ion irradiations resulted in three observations: 1) the average values of KAM increased; 2) maximum values of KAM increased; 3) the range of KAM values increased, as compared to the corresponding unirradiated samples. Hence, the graphs for the irradiated samples shifted to the right (observation 1 and 2) and expanded (observation 3).

3.4. Film thickness verification and stability of the film-substrate interface

The purpose of the SIMS study performed for samples SN553* and SN554 was: 1) to verify the film thickness obtained from the dual beam measurement for sample SN553*; 2) to verify the assumption that the films deposited for the same amount of time under similar conditions have the same thickness; 3) to examine the effect of ion irradiation on mixing at the film-substrate interface.

A plot of the SIMS results for U-Zr pair (U is the film element, Zr is the substrate element) for samples SN553* and SN554 is shown in Fig. 11. The film thickness can be estimated by drawing a tangent at the point where the most rapid increase in the relative percentage of sputtered Zr ions occurs. The estimation shows that the film thickness for both samples is ~160 nm. This is in good agreement with the film thickness of ca. 150 nm measured by the dual beam method for sample SN553*. This also indicates that the assumption that the films deposited for the same amount of time under similar conditions have the same thickness is valid and no significant sputtering during U ion irradiation took place. The relative shapes of the U and Zr curves for samples SN553* and SN554 indicate that the irradiation with 110 MeV U ions to a fluence of 5×10^{11} ions/cm^2 did not cause any significant elemental mixing at the film-substrate interface, as compared to the unirradiated

sample. The undulated shape of the U curve between 0 and 100 nm for irradiated sample SN553* suggests that the U distribution in the film becomes less uniform, as compared to the unirradiated case.

4. Discussion

Carbonaceous contamination layer on the film surfaces, most likely, is originating from the adsorption of atmospheric CO_2 and oil vapour from vacuum pumps used in the SEM, EBSD and XPS instruments. The UO_2 surface becomes heavily charged under the electron beam irradiation and this facilitates oil vapour deposition.

Particulate contamination more likely comes from the deposits on the walls of the film growing chamber. The contaminant particle composition (U, Nb, Ta) supports this explanation (tantalum target and Nb wire heating element were used in that chamber). It is possible to suggest that these contamination particles might act as local catalytic sites – they might increase or decrease corrosion of the UO_2 film in the vicinity.

Unfortunately, it was impossible to observe the nano-scale grains for the corresponding unirradiated samples due to severe surface charging, but it is expected that the unirradiated samples also have the nano-scale structure in the same way as samples SN553* and SN554 have the nano-scale ripple structure. A speculative suggestion can be made that the formation of this nano-structure is caused by the compression stress in the UO_2 film due to the lattice parameter mismatch between the UO_2 film and the substrate. Hence, the observed elongated grains and ripples can be seen as the film folds that accommodate the strain, thus relieving the unit cells from the compressive strain. Hence, single crystal UO_2 can grow on YSZ substrates despite the 6.4% lattice mismatch.

The fact that the irradiated samples showed less surface charging can possibly be explained by an increase in the UO_2 conductivity as a result of the defects produced by the ion irradiations. An increase of electrical conductivity and surface area due to hillock structures might increase dissolution of the UO_2 matrix [16]. Hence, dissolution experiments to test this hypothesis can be suggested.

The XRD and EBSD results indicate that sputtering of UO_2 onto YSZ substrates results in epitaxial growth of UO_2 films, where UO_2 matches the crystallographic orientation of YSZ substrates. Based on the expected epitaxial relationship for UO_2 films on YSZ substrates and the obtained results from the XRD and EBSD studies it possible to suggest that the UO_2 films on the YSZ substrates can be considered as single crystals. However, in-plane φ XRD scans should be conducted to verify a single growth domain, as was described by Strehle et al. [17]. Uranium dioxide films on (0 0 1) YSZ substrates, produced under similar conditions, were thoroughly characterised by Strehle et al. [17] and it was shown that these films were single crystals.

The observed peak broadening in the XRD study is caused by the size reduction of coherent crystallite domains and microstrain induced by the ion irradiation. A shift in 2θ position arises from variation in the lattice plane separation caused by the ion irradiation. Shift towards lower values of 2θ observed for most of the cases indicates increase in the lattice plane separation (unit cell swelling), which is the expected response to radiation damage [27]. Shift towards higher values of 2θ observed for UO_2 reflections in sample SN556*, indicating lattice contraction, was rather unexpected. A possible explanation for the observed lattice contraction can be that the extended network of ion tracks caused the compression of the film resulting in individual unit cell contraction. Alternatively, the ion irradiation could induce Zr incorporation from the substrate into the UO_2 film. Zirconium ions are partially soluble in the UO_2 lattice and are known to cause significant lattice contraction [28].

The observation that sample SN553* with UO_2 film in (1 1 0) crystallographic orientation, irradiated to a fluence a factor of 10 less than sample SN556* with UO_2 in (1 1 1) orientation, has a larger value of average KAM (0.8°) than sample SN556* (0.7°) suggests that (1 1 1) crystallographic plane of UO_2 is more resistant to ion impact than (1 1 0) plane. In addition, the HS-AFM study shows that sample SN553* has both higher RMS roughness value and relative increase in roughness, as compared to its corresponding unirradiated sample than sample SN556*. The observation that different crystallographic orientations have different ion irradiation stability was noted by others. For example, work by Usov et al. [29] reports that different crystallographic orientations of single crystal YSZ (fluorite type structure) showed different irradiation tolerances. Liu et al. [30] reported the same observation for grains with different crystallographic orientation in polycrystalline tungsten. This observation allows proposing that grains with different crystallographic orientations in polycrystalline UO_2 matrix of real nuclear fuel will have different response to radiation damage by fission fragments. As a result, spent nuclear fuel will have grains with lower or higher structural and chemical stability due to fission damage. This observation shows that real spent nuclear fuel is a complicated heterogeneous system and highlights difficulties in its characterisation.

5. Conclusions

Uranium dioxide undergoes epitaxial growth on single crystal YSZ substrates during which it adopts the crystallographic orientations of the substrate. The YSZ substrates with (0 0 1), (1 1 0) and (1 1 1) crystallographic orientations were used in this work.

Further work is required to understand the mechanism that is responsible for formation of such a complex nano-structure that is presented by nano-scale grains and ripples.

Low irradiation fluences with uranium ions ($\leqslant 5 \times 10^{12}$ ions/cm^2) are not sufficient to cause any significant changes to the crystallographic orientation. However, the effect of the induced radiation damage can be quantified in terms of kernel average misorientation. It was observed that the irradiated samples have a higher value of KAM than the corresponding unirradiated samples.

Despite the lack of a direct comparison between UO_2 film orientations irradiated with the same fluence, the uranium dioxide (1 1 1) plane showed a higher irradiation tolerance, as characterised by its lower average value of KAM and RMS roughness, than the (1 1 0) plane irradiated at a lower fluence.

The UO_2 film-YSZ substrate interface is stable with respect to elemental mixing even under irradiation with 110 MeV U ions to a fluence of 5×10^{11} ions/cm^2, as compared to the corresponding unirradiated sample.

Supporting data

Supporting data will be available in A.J. Popel's PhD thesis (University of Cambridge) published online.

Acknowledgements

The irradiation experiment was performed at the Grand Accélérateur National d'Ions Lourds (GANIL) Caen, France, and supported by the French Network EMIR. Thanks are given to the CIMAP-CIRIL staff and the GANIL technical staff, especially, T. Madi and F. Durantel for the technical support during the experiments.

A.J. Popel acknowledges funding from the UK EPSRC (grant EP/I036400/1) and Radioactive Waste Management Ltd (formerly

the Radioactive Waste Management Directorate of the UK Nuclear Decommissioning Authority, contract NPO004411A-EPS02).

References

[1] N. Ishikawa, Y. Chimi, O. Michikami, Y. Ohta, K. Ohhara, M. Lang, R. Neumann, in: Nucl. Instr. Meth. Phys. Res. B 266 (2008) 3033–3036.
[2] Hj. Matzke, P.G. Lucuta, T. Wiss, in: Nucl. Instr. Meth. Phys. Res. B 166-167 (2000) 920–926.
[3] T. Wiss, Hj. Matzke, C. Trautmann, M. Toulemonde, S. Klaumünzer, in: Nucl. Instr. Meth. Phys. Res. B 122 (1997) 583–588.
[4] V.G. Baranov, A.V. Lunev, V.F. Reutov, A.V. Tenishev, M.G. Isaenkova, A.V. Khlunov, J. Nucl. Mater. 452 (2014) 147–157.
[5] F. Garrido, L. Nowicki, L. Thomé, in: Nucl. Instr. Meth. Phys. Res. B 240 (2005) 250–257.
[6] F. Garrido, C. Choffel, J.-C. Dran, L. Thomé, L. Nowicki, A. Turos, in: Nucl. Instr. Meth. Phys. Res. B 127/128 (1997) 634–638.
[7] P.B. Weisensee, J.P. Feser, D.G. Cahill, J. Nucl. Mater. 443 (2013) 212–217.
[8] P.D. Edmondson, Y. Zhang, S. Moll, F. Namavar, W.J. Weber, Acta Mater. 60 (2012) 5408–5416.
[9] T. Sonoda, M. Kinoshita, N. Ishikawa, M. Sataka, A. Iwase, K. Yasunaga, Nucl. Instr. Meth. Phys. Res. B 268 (2010) 3277–3281.
[10] Hj. Matzke, J. Spino, in: J. Nucl. Mater. 248 (1997) 170–179.
[11] M. Kinoshita, K. Yasunaga, T. Sonoda, A. Iwase, N. Ishikawa, M. Sataka, K. Yasuda, S. Matsumura, H.Y. Geng, T. Ichinomiya, Y. Chen, Y. Kaneta, M. Iwasawa, T. Ohnuma, Y. Nishiura, J. Nakamura, Hj. Matzke, Nucl. Instr. Meth. Phys. Res. B 267 (2009) 960–963.
[12] A. Iwase, H. Ohno, N. Ishikawa, Y. Baba, N. Hirao, T. Sonoda, M. Kinoshita, Nucl. Instr. Meth. Phys. Res. B 267 (2009) 969–972.
[13] H. Ohno, A. Iwase, D. Matsumura, Y. Nishihata, J. Mizuki, N. Ishikawa, Y. Baba, N. Hirao, T. Sonoda, M. Kinoshita, Nucl. Instr. Meth. Phys. Res. B 266 (2008) 3013–3017.
[14] Hj. Matzke, Nucl. Instr. Meth. Phys. Res. B 65 (1992) 30–39.
[15] H. He, Z. Qin, D.W. Shoesmith, Electrochim. Acta 56 (2010) 53–60.
[16] Hj. Matzke, in: J. Nucl. Mater. 190 (1992) 101–106.
[17] M.M. Strehle, B.J. Heuser, M.S. Elbakhshwan, X. Han, D.J. Gennardo, H.K. Pappas, H. Ju, Thin Solid Films 520 (2012) 5616–5626.
[18] Z. Bao, R. Springell, H.C. Walker, H. Leiste, K. Kuebel, R. Prang, G. Nisbet, S. Langridge, R.C.C. Ward, T. Gouder, R. Caciuffo, G.H. Lander, Phys. Rev. B 88 (2013) 134426.
[19] R.C.C. Ward, R.A. Cowley, N. Ling, W. Goetze, G.H. Lander, W.G. Stirling, J. Phys.: Condens. Matter 20 (2008) 135003.
[20] J.F. Ziegler, J.P. Biersack, M.D. Ziegler, The Stopping and RANGE of Ions in Matter, SRIM Co., Chester, Maryland, U.S.A., 2008.
[21] P. Klapetek, L. Picco, O. Payton, A. Yacoot, M. Miles, Meas. Sci. Technol. 24 (2013) 025006.
[22] O.D. Payton, L. Picco, D. Robert, A. Raman, M.E. Homer, A.R. Champneys, M.J. Miles, Nanotechnology 23 (2012) 205704.
[23] D.W. Shoesmith, S. Sunder, J. Nucl. Mater. 190 (1992) 20–35.
[24] Y.A. Teterin, A.J. Popel, K.I. Maslakov, A.Y. Teterin, K.E. Ivanov, S.N. Kalmykov, R. Springell, T.B. Scott, I. Farnan, Inorg. Chem. 55 (2016) 8059–8070.
[25] S.I. Wright, M.M. Nowell, D.P. Field, Microsc. Microanal. 17 (2011) 316–329.
[26] L. Saraf, Microsc. Microanal. 17 (2011) 424–425.
[27] N. Nakae, A. Harada, T. Kirihara, J. Nucl. Mater. 71 (1978) 314–319.
[28] J. Cobos, D. Papaioannou, J. Spino, M. Coquerelle, J. Alloys Compd. 271–273 (1998) 610–615.
[29] I.O. Usov, S. Rubanov, J. Won, A.A. Suvorova, Nucl. Instr. Meth. Phys. Res. B 326 (2014) 283–288.
[30] F. Liu, H. Ren, S. Peng, K. Zhu, Nucl. Instr. Meth. Phys. Res. B 333 (2014) 120–123.